Available online at www.sciencedirect.com

ScienceDirect

Solar Energy 116 (2015) 257–264

SOLAR ENERGY

www.elsevier.com/locate/solener

# Evidence of plasmonic effects in random orientation silver nanowire meshes on silicon

Ross Jarrett [a,*], Hiroyuki Kanda [b], Norihisa Harano [b], Takuma Noguchi [b], Rolf Crook [a], Seigo Ito [b]

[a] Energy Research Institute, University of Leeds, Leeds LS2 9JT, United Kingdom
[b] University of Hyogo, 2167 Shosha, Himeji 671-2201, Japan

Received 2 October 2013; received in revised form 13 March 2015; accepted 6 April 2015

Communicated by: Associate Editor Elias K. Stefanakos

**Abstract**

In this work silver nanowires were used as the transparent conductive electrode on a crystalline silicon solar cell in place of the commonly used screen printed grid. Light transmission and surface characterisation of the cells displays an average of 22% more light transmission than the physical non-AgNW shaded area of the cell surface. Further to this it is observed that plasmonic effects result in an increased scattering of incoming light into the cell, which also reduced the amount of light reflected from the cell's front plane. The cells with silver nanowire electrodes did not, however, show improved current–voltage characteristics compared to cells without a front electrode. This is attributed to the overall low light transmission as a result of silver nanoparticles present in the electrodes and poor electrical connection between silicon cell and electrode. Finally, a large reduction in the mass of silver used for the nanowire electrodes was observed when compared to standard screen printed grid fingers.


*Keywords:* Silver nanowires; LSPR; Scattering; TCE

## 1. Introduction

Silicon cell prices have shown a large reduction in recent years due to the reduction in silicon manufacturing costs and market forces. One area of solar cell cost reduction that can still be addressed is the silver grid on the front face of silicon solar cells. A mixture of silver (~70–85%), glass frits, cellulose resin, a solvent and other trace additives are commonly Screen Printed (SP) to produce the grid (Caballero, 2010). However, this can suffer from high shading losses and low fill factors due to junction shunting and series resistance from contact resistance and low metal conductivity (Hilali et al., 2004). Whilst other higher efficiency methods such as buried contacts and photolithography can be used these add manufacturing expense (Wohlgemuth et al., 1990).

Silver nanowires (AgNWs) could offer a lower cost alternative front electrode by reducing the mass of silver used. AgNWs can be produced in either template or chemical synthesis methods (Han et al., 2000; Rowell et al., 2006; Tung et al., 2009; Govindaraj et al., 2000; Hong et al., 2001; Braun et al., 1998; Jana et al., 2001; Murphy and Jana, 2002; Kang and Guo, 2007; Zhou et al., 1999; Caswell et al., 2003; Hu et al., 2004). A common chemical

* Corresponding author.
*E-mail addresses:* pmrjj@leeds.ac.uk (R. Jarrett), er13u019@steng.u-hyogo.ac.jp (H. Kanda), er12j042@steng.u-hyogo.ac.jp (N. Harano), er13j043@steng.u-hyogo.ac.jp (T. Noguchi), R.Crook@leeds.ac.uk (R. Crook), Itou@steng.u-hyogo.ac.jp (S. Ito).

http://dx.doi.org/10.1016/j.solener.2015.04.009
0038-092X/

synthesis is the salt mediated polyol synthesis which is able to produce high aspect nanowires in a one-pot ambient soft-solution process (Korte et al., 2008). This is a low cost method to manufacture large quantities of AgNWs.

AgNW meshes have been demonstrated as a transparent conductive electrodes (TCE) in cells with low active layer mobility, such as organic solar cells, in place of the traditionally used transparent conductive oxide (TCO) (Morgenstern et al., 2011; Gaynor et al., 2009). They have also been demonstrated with some amorphous silicon and hybrid organic-silicon cells (Chen et al., 2012a; Chen et al., 2012b). AgNWs, however, have yet to be used with a p–n crystalline silicon junction which, due to its high mobility top layer, could potentially not necessitate the same resistivity reduction as low mobility substrate cells.

Other potential benefits of AgNW meshes could be achieved from plasmonic effects. Localised Scattering Plasmon Resonances (LSPR) are collective oscillations of the conduction electrons. The oscillating dipole produced by the electron oscillation re-radiates light at the same frequency resulting in scattering (Hutter and Fendler, 2004). This effect is observed in noble metal nanoparticles, with resonant frequency and scattering cross section affected by size, shape and dielectric environment (Underwood and Mulvaney, 1994). LSPR may therefore enable a larger transmission percentage compared to the physical shading of the mesh (van de Groep et al., 2012).

In this work AgNWs were synthesised using the salt mediated polyol process and, after extraction, were deposited onto glass and $POCl_3$ gas doped n-type silicon. *I–V* curves, sheet resistance ($R_{sheet}$) and light transmission/reflection of the samples was compared before and after deposition to quantify the optical end electrical effects of using a silver nanowire TCE.

## 2. Experimental

The silicon wafers were cut to $2.5 \times 2.5\,cm^2$ square pieces from 6-in. mono crystalline silicon wafers. One surface was as cut, and the other was polished as a mirror, (purchased from RS Technologies, Japan). The wafers are first cleaned by RCA method. The chemicals used were $NH_3$, (28–30%, Kanto Chemical Co. Ltd., Japan), HCl, (35–37%, Kishida Chemical Co. Ltd, Japan), $H_2O_2$, (35%, Tokyo Chemical Industry Co. Ltd., Japan), HF, (46%, Wako Pure Chemical Industries, Ltd., Japan), and $HNO_3$, (60%, Kishida Chemical Co. Ltd., Japan). As per the RCA cleaning method, the silicon wafers were washed by a HF solution ($HF:H_2O = 1:9$, v/v) at room temperature for 1 min, a $NH_3$ solution ($NH_3:H_2O_2:H_2O = 1:1:5$, v/v/v) at 80 °C for 20 min, a HCl solution ($HCl:H_2O_2:H_2O = 1:1:5$, v/v/v), and a HF solution ($HF:H_2O = 1:9$, v/v) at room temperature for 1 min again. Between each treatment above, the wafers were rinsed by water. The n+ emitters were obtained with heat treatments at 925 °C for 30 min with $N_2$ flow, (0.1 l per minute,) through a $POCl_3$ bubbler, (99%, Kishida Chemical Co. Ltd., Japan) in quartz tubular oven, (internal diameter: $\phi$ 46 mm.) The resulting phosphosilicate glass (PSG) was removed by the 10% HF etch for 1 min. Protecting the n+ emitter layer by masking tape on the mirror polished side, the backside, (as-cut side), phosphate-doped layer was etched by a HF solution, ($HF:HNO_3 = 0.75:5$, v/v) at room temperature for 3 min and rinsed by water. After the removal of the masking tape, aluminium electrodes were formed on the back side by screen printing aluminium paste, ($1.5 \times 1.5\,cm^2$ square, Noritake, Japan), drying at 125 °C for 10 min, and annealing at 800 °C for 1 min in air.

AgNW were synthesised as detailed by Korte et al. (2008). The as synthesised AgNW solution was diluted to 10 times its original volume with acetone and placed in an ultrasonic bath for 10 min to disperse the synthesis product. The solution was then centrifuged at 2000RPM for 20 min followed by pipetting off the supernatant. This process was repeated a further four times.

The as extracted nanowire samples were deposited on 1 $cm^2$ areas of glass and silicon solar cells which had been masked off. The samples were spin-cast by addition of 20 µl drops of AgNW solution added followed by spinning at 2000RPM for 15 s. 3 different coverage densities were achieved by repeating the deposition 15, 18 and 21 times. Three samples were produced at each density on both glass substrates, (G15, G18, G21) and silicon cells, (Si15, Si18, Si21) to provide insight into variation in the processes.

Samples were annealed under ambient atmosphere for 20 min at 180 °C to evaporate off any remaining solvent and sinter wire junctions to reduce the overall sheet resistance.

The power of an AM 1.5 solar simulator (100 mW $cm^{-2}$, YSS-80, Yamashita Denso, Japan) was calibrated using a reference silicon photodiode (Bunkou Keiki, Japan). The photo current–voltage curves were obtained by the application of an external bias to the cell and by measuring the generated photocurrent with a digital source meter. The front contact was performed by pressing spring probe needles to the n+ emitter surface. The microstructures of the AgNW layers were viewed by scanning electron microscopy (SEM; JSM-65110, JEOL). Reflecting absorption spectra were measured by an UV–vis spectrometer (Lambda 750 UV–vis Spectrometer, Perkin–Elmer).

## 3. Results and discussion

### 3.1. Synthesised nanowires

Nanowires synthesised by the $CuCl_2$ mediated polyol process are shown deposited on the silicon cell in Fig. 1. Wires synthesised using this method have a measured mean length of $4.3 \pm 0.4$ µm and $64 \pm 2$ nm mean width. A large number of silver nanoparticles are observed to be deposited on the silicon cell in Fig. 3. These particles are produced as a result of the thermodynamics of the wet synthesis method (Sun et al., 2002). The centrifuge method aimed at separating these particles from the wires is seen to have poor

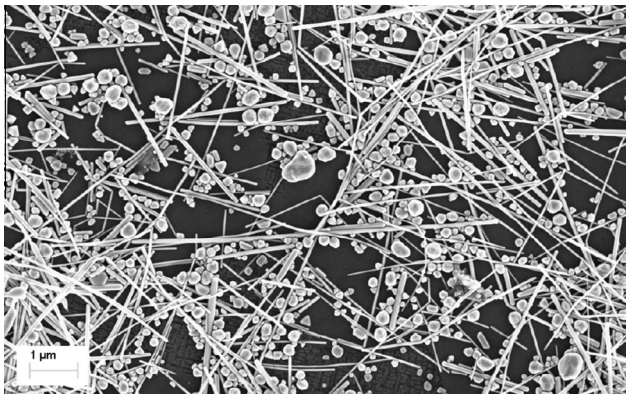


Fig. 1. Vertical SEM image of 15 drop silicon cell.

results, which is likely to result in reduced transmission and higher sheet resistances of the resultant samples.

### 3.2. Sheet resistance

The Sheet resistances of the AgNW on glass and the silicon cells, before and after AgNW deposition, were obtained using a 4-point probe, shown in Fig. 2.

The expected reduction in $R_{sheet}$ with increasing nanowire mass is clearly observed for the glass samples reducing from $34 \pm 4\ \Omega/\square$ for the G15 sample to $18 \pm 1\ \Omega/\square$ for the G21 sample. The silicon cells without a nanowire mesh were observed to have $R_{sheet} = 28 \pm 2\ \Omega/\square$. With the addition of the lowest density of nanowires a large reduction in surface sheet resistance is observed, reducing to $R_{sheet} = 18 \pm 1\ \Omega/\square$. As the nanowire density is increased to 18 drops with the Si18 sample no decrease in sheet resistance is observed. Further increase of AgNW density shows a similar reduction in sheet resistance as the same density mesh glass samples.

### 3.3. Optical transmission and reflection

#### 3.3.1. Optical transmission

Optical transmission for the three nanowire densities deposited on glass are shown in Fig. 3. All three densities

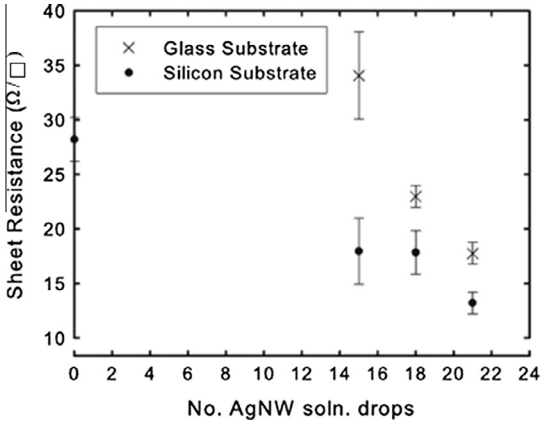


Fig. 2. Sheet resistance values measured for AgNW deposited on glass and top surface of silicon cell.

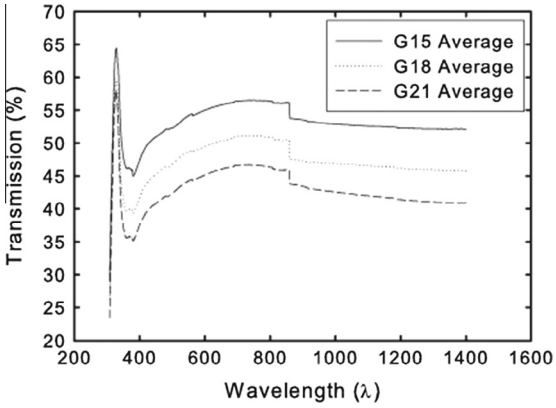


Fig. 3. Light transmission of different density AgNW meshes deposited on borosilicate glass slides.

show qualitatively similar transmission behaviour over the wavelength range with reducing transmission observed for increasing nanowire density. A reduction in transmission is observed from ~700 nm resulting in a minima at ~390 nm with a shoulder and secondary minima at ~365 nm observed.

Reduced transmission of the nanowire samples is attributed to LSPRs of both wires and the remnant nanoparticles. Previous studies have calculated the extinction peaks for 100 nm silver spheres in a vacuum to be 393 nm for dipolar excitations and 354 nm for quadrupolar excitations, with a red shift, and increasing order oscillations for larger particles. For those particles in a medium with a higher refractive index than air, such as silicon, it is also observed for the peak extinction wavelength to redshift (Temple et al., 2009). When semi-spherical particles are produced on silicon substrates with a mean particle diameter of 60.4 nm broad transmission extinction peaks are observed with minima at 429 nm and 355 nm, with redshifting observed for larger distribution mean diameters (Temple et al., 2009). Simulations by Kottman et al. have calculated extinction peaks for 20 nm diameter silver nanowires at 357 nm, with a redshift observed for larger width wires (Kottmann and Martin, 2001).

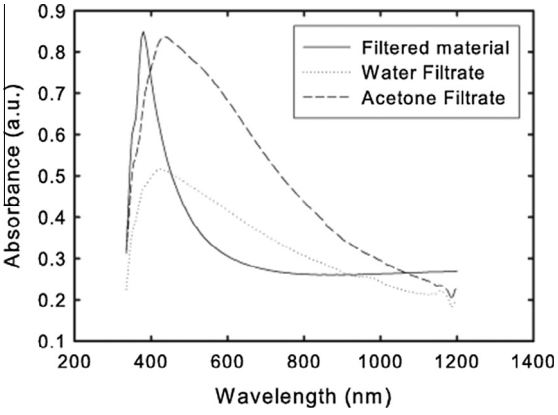


Fig. 4. Absorbance of filtered material composed of largely nanowires and filtrate materials composed largely of nanoparticles and low aspect ratio nanowires.

Table 1
Area of cell substrate uncovered for Si15, Si18 and Si21 samples.

| Nanowire volume deposited ×20 (μl) | Percentage area of cell uncovered (%) |
|---|---|
| 15 | 31 ± 2 |
| 18 | 22 ± 2 |
| 21 | 21 ± 1 |

Fig. 4 shows the absorbance of AgNWs, and nanoparticles separated by a multi-pass filtration method. The separated nanowires, measured to contain 14 ± 3% nanoparticles, shows absorbance peaks at 380 nm and 355 nm. Whilst the acetone and water filtrate, containing largely particulate and short aspect wire matter, shown in Fig. 4 have peak absorptions at higher wavelengths. From this data it is understood that the minima at 390 nm is attributed to the LSPRs of the silver nanowires and the shoulder and secondary minima at 365 nm relating to the AgNWs and nanoparticles quadrupolar extinction. The broad reduction to the extinction peak at 390 nm is thought to relate to the diameter distribution of the AgNWs and the dipolar extinction peak of the nanoparticles.

The light transmission of these samples is observed to be low when compared to grid shading ratios normally achieved from SP silver grids. However, if the transmission is compared to the actual shading by the wires when observed in vertical perspective SEM images, shown in Fig. 1, a large increase in transmission is observed. The maximum non-AgNW shaded area on the silicon cells, shown for the three AgNW densities in Table 1, is 31 ± 2% for the Si15 sample whilst the average transmission from 1200 nm to 330 nm for the same density sample on glass is 53.4 ± 0.1% showing a 22% increase in transmission over the shaded area, which is transmitted by scattering within the mesh.

### 3.3.2. Light reflection

The silicon cells used in this study had no top layer texturing to reduce light reflection. Such cells suffer from a large percentage of light reflection. The reflectance measured for the bare silicon cells and the cells with AgNW meshes are shown in Fig. 5.

From Fig. 5 it is seen that very different reflection behaviour occurs upon the addition of AgNW to the silicon cells. It is observed that the reflection of the nanowires is greater than silicon above ~745 nm. In this region the reflection of the nanowires is seen to be greater for the more dense networks. Previous investigations into plasmonics attributed a sharp cut-off in the transverse electric field at ~750 nm in optically thick, i.e. thicker than the skin depth of metal (~10 nm in silver,) metal grids (Catrysse and Fan, 2010; van de Groep et al., 2012). This results in slightly reduced transmission, and thus greater reflection, above this value as the transverse magnetic mode propagation is still supported (Catrysse and Fan, 2010; van de Groep et al., 2012). This transmission decrease above

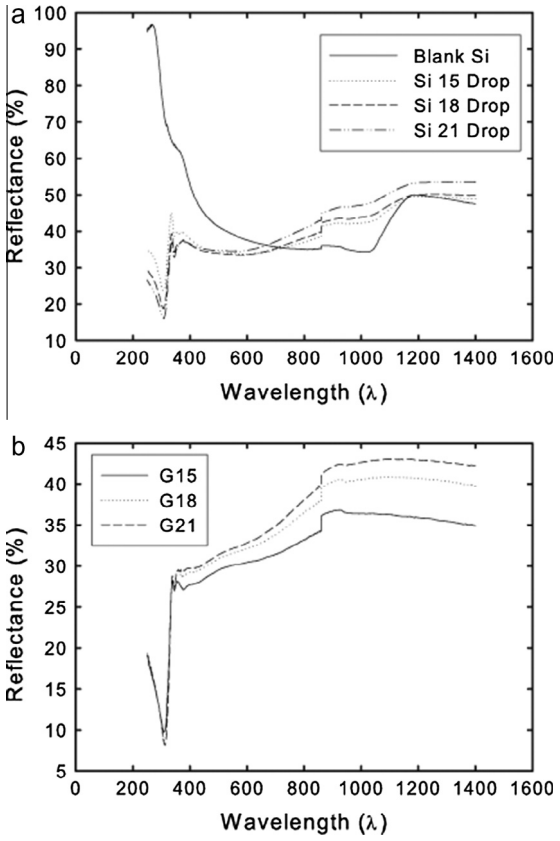


Fig. 5. Reflectance percentages for (a) bare silicon cells and cells with AgNW deposited. (b) AgNW deposited on glass substrates.

750 nm is observed in Fig. 3 and from Fig. 5 also appears to result in an increase in reflectance. A further increase in reflectance with AgNW density supports this theory.

Below approximately 750 nm the converse is observed with lower reflection from the AgNW samples. A transition is also observed with regards to the most and least reflecting samples with the least dense meshes observed to be reflecting a larger percentage of light than the denser meshes. This wavelength range is that where the LSPR occurs in the samples and as such reduced reflection could be attributed to either an increased absorption by the nanowires in this wavelength range, or it could also be considered that the light is scattered by the meshes at the LSPR frequency. This light can be preferentially forward scattered into the substrates as has previously been observed (Catchpole et al., 2008). When considering the forward scattering of the nanowires it is found to be dependent on the local density of optical states (LDOS), as these are observed to be high in the silicon it could be considered that this change in reflectance with regards to the density of nanowire coverage of the silicon could be due to more forward scattering by the nanowires on the silicon cells. This theory is supported when the reflectance of the samples when deposited on glass, which has a lower LDOS, is observed shown in Fig. 5. In the glass samples it is observed that the most dense nanowire sample is seen to reflect the most.

Reflectance data of silver nanoparticles on silicon from Temple et al. observed a minima for the quadrupolar excitation at 373 nm and a maxima for the dipolar excitation at 550 nm where the dipolar maximum indicates substrate influence on the angular distribution of the scattered light (Temple et al., 2009). Although a large number of particles were present on the samples produced in this study, similar features were not observed. It is unknown whether this is due to the different particle size and environment, or due to the response of the nanoparticles being hidden by the AgNW.

### 3.4. Incident photon to current efficiency

To assess the effects of the AgNWs plasmonics on a cell level the Incident Photon to Current Efficiency (IPCE) was performed on the Si0, Si15, Si18 and Si21 cells, shown in Fig. 6. It is clear that the Si0 cell shows a higher IPCE over all wavelengths when compared to the cells with AgNW meshes, which show reducing IPCE with increasing AgNWs. This is expected due to the reduced incident light transmission when AgNW meshes are present. A small peak is observed in the AgNW EQE spectra at ≃390 nm. When the Si15, Si18 and Si21 IPCE spectra are normalised to the Si0 in Fig. 6, showing the major differences between the cells with and without AgNW, the peak is enhanced and which is attributed to the LSPR of the AgNW.

Similarly to the transmission spectra, a reducing ICPE from wavelengths below ≃700 nm is also seen which is an attribute of either the AgNW or the nanoparticles present. This is likely caused by LSPR that results in parasitic absorption of the incident light rather than scattering. Parasitic absorption could be exacerbated by the presence of the large quantity of AgNW and nanoparticles away from the silicon surface, which will scatter light in all directions. This could be linked to the reflection results where reduced reflection is caused by multiple instances of incident light being absorbed, scattered and reabsorbed resulting in overall absorption losses in the AgNW and nanoparticles. It is possible that these parasitic absorptions could be reduced by utilising less AgNWs and efficiently removing nanoparticles so that light is more effectively coupled into the cell. Finally a reduction in IPCE is also observed in the red region which is likely attributed to reflection of light from the AgNWs. Overall this suggests that the LSPR of the AgNWs have the potential to provide photocurrent enhancement, but it is necessary to reduce parasitic absorption from nanoparticles and excess AgNWs.

### 3.5. IV Curves

For AgNW electrodes deposited on silicon cells it is important to consider the light transmitted to the substrate and the series resistance, $R_{series}$. They can also be further tested for factors that they must avoid such as shunting the cell. The optimum $IV$ curves achieved for the bare

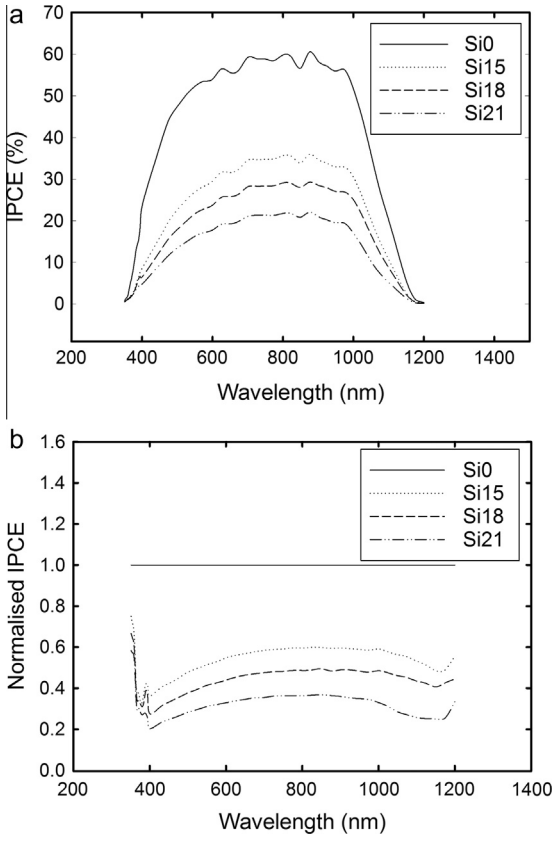


Fig. 6. (a) IPCE values for Si0, Si15, Si18 and Si21 cells. (b) IPCE normalised to that of Si0.

silicon cell, Si0, and the Si15, Si18, Si21 cells are shown in Fig. 7 alongside the average measurements over 3 cells in Table 2.

All cells have a similar $V_{oc}$ as expected but with a reduced $I_{sc}$ with increasing AgNW density which can be attributed to the reducing transmission. One important measure of the AgNW meshes performance is the series resistance, $R_{series}$, of the cell. This accounts for the resistance of the mesh but also other factors such as the mesh connectivity with the cell substrate (Caballero, 2010). The Si0 and Si15 cells both show similar values of $12 \pm 2\ \Omega\,cm^2$ and $11 \pm 1\ \Omega\,cm^2$ respectively. However, the Si18 and Si21 cells show greatly increased series resistance of $51 \pm 6\ \Omega\,cm^2$ and $66 \pm 17\ \Omega\,cm^2$ both of which suggest poor electrical properties with AgNWs, further confirmed by the same poor fill factor of $0.27 \pm 0.01$.

The increase in $R_{series}$ of the Si18 and Si21 samples is counter to the expected reduction that would be assumed to occur with their reducing $R_{sheet}$ values. This increase in $R_{series}$ could be attributed to the 3D nature of the mesh and the dimensionally different measurements taken by $R_{sheet}$ and $R_{series}$ measurements. $R_{sheet}$ measurements are taken using a 4 point probe across the top surface of the mesh, whilst $R_{series}$ measurements are taken through the entirety of the cell and thus vertically through the nanowire mesh. If we consider the mesh as shown in Fig. 8 we can consider how its 3 dimensional nature evolves with

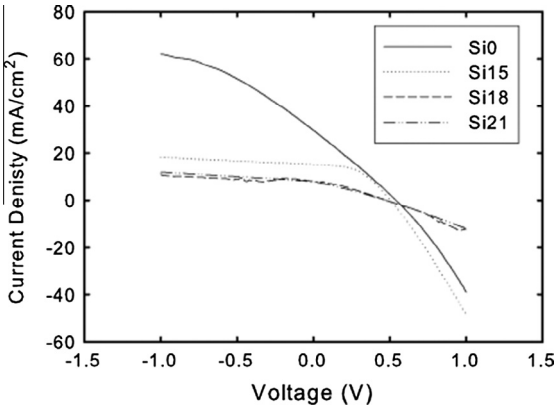


Fig. 7. *IV* curves for pn silicon cells with; no nanowires, 15 drop AgNW mesh, 18 drop AgNW mesh, 21 drop AgNW mesh.

increased concentration and the different measurements and their outcomes. When the sheet resistance and series resistance for the Si15 sample are measured both measurements are measuring $R_{high}$ the resistance of the nanowire mesh adjacent to the substrate. With the addition of more nanowire solution two possible scenarios could occur: 1. the additional nanowires and nanoparticles form a layer of nanowires on top of the first layer, 2. The nanowires of the additional nanowire solution form an upper layer above first layer and the additional nanoparticles pass through the mesh adding to the nano-mesh in the region close to the substrate. In both of these scenarios a measurement of the sheet resistance will only measure the upper layer percolation paths which can potentially have a reduced resistance, $R_{low}$. However, a series resistance measurement will measure a resistance path vertically through both the $R_{high}$ mesh adjacent to the substrate and the upper layer, $R_{low}$, mesh as well as any one of a large number of connecting paths, $R_{connect}$, between $R_{high}$ and $R_{low}$. This resistance could be much higher than the upper layer $R_{low}$ path due to possibly having a larger number of junctions and potentially due to an increased number of low aspect nanowires of nanoparticles present in the substrate adjacent $R_{high}$ layer.

The Si0 cell with no front electrode shows poor IV characteristics with a low fill factor of $0.26 \pm 0.01$ and an apparent low $R_{shunt}$ of 19 Ω. This low fill factor can be attributed to a high $R_{series}$ which has flattened the entire IV curve. The $R_{shunt}$ is calculated from the gradient of the IV curve at $I_{sc}$ which has also been influenced by the high $R_{series}$. In reality, the $R_{shunt}$ of Si0 is likely to be similar to that of Si15 at 1000 Ω. The apparent $R_{shunt}$ of Si18 and Si21 may have been similarly reduced due to high $R_{series}$. The Si15 cell shows an improved IV curve and has an accurate $R_{shunt}$ measurement due to it having a reduced substrate illumination, due to poor transmission through the dense AgNW mesh, when compared to the Si0 cell and lower $R_{series}$ compared to the Si15 and Si18 samples. This also translates to an improvement in the fill factor of the Si15 cell of $0.46 \pm 0.03$.

These results and potential explanation suggests two things to be considered to improve the results: 1. AgNWs need to be deposited at different concentrations so that a lower conductivity mesh is achieved whilst also achieving a proportional increase in surface coverage. 2. There is a maximum nanowire density at which optimal properties are achieved beyond which a reduction in cell efficiency is observed. This second point could be attributed to both properties of the AgNWs themselves, but also to modelling efforts used to determine optimum finger separation distance for SP grids which is dependent on the $J_{sc}$ and $V_{oc}$ (Caballero, 2010).

### 3.6. Mass of silver used

One of the primary reasons for investigating AgNW electrodes is the reduction in silver mass to reduce silicon cell cost. Table 3 shows the volume of silver in typical SP electrodes and the volume of the silver nanowires and nanoparticles on the Si15 cell. The volume of silver for the SP grids was calculated for typical fingers 14 μm tall, 80 μm wide with a separation of 0.2 cm (Hilali et al., 2004; Caballero, 2010). Volume of silver for Si15 cells were calculated using the SEM images of coverage and previously collected nanowire and nanoparticle statistics for nanowires produced in the salt mediated polyol process.

The total volume of silver deposited on the Si15 sample is $0.15 \pm 0.01$ cm$^3$ which is slightly over a quarter of the SP grid volume of 0.56 cm$^3$. This value for the nanowire electrode contains particles, which previous studies have accounted to total ~35%. These particles are detrimental to the performance of the electrode and if removed would

Table 2
Current density, voltage, power, fill factor, resistance and efficiency values for Si0, Si15, Si18 and Si21.

| | Si0 | Si15 | Si18 | Si21 |
|---|---|---|---|---|
| $J_{sc}$ (mA/cm$^2$) | $29.3 \pm 0.3$ | $14.2 \pm 0.5$ | $7.7 \pm 0.5$ | $5.2 \pm 1.4$ |
| $V_{oc}$ (V) | $0.52 \pm 0.02$ | $0.49 \pm 0.01$ | $0.48 \pm 0.01$ | $0.49 \pm 0.01$ |
| $P_{max}$ (mW/cm$^2$) | $4.1 \pm 0.2$ | $3.2 \pm 0.2$ | $1.00 \pm 0.03$ | $0.7 \pm 0.2$ |
| $V_{max}$(V) | $0.272 \pm 0.008$ | $0.295 \pm 0.008$ | $0.241 \pm 0.006$ | $0.25 \pm 0.01$ |
| $I_{max}$ (mA/Cm$_2$) | $15.0 \pm 0.1$ | $10.9 \pm 0.3$ | $4.1 \pm 0.2$ | $2.8 \pm 0.8$ |
| Fill factor | $0.26 \pm 0.01$ | $0.46 \pm 0.03$ | $0.27 \pm 0.01$ | $0.27 \pm 0.01$ |
| $R_{series}$(Ω cm$^2$) | $11 \pm 1$ | $11 \pm 1$ | $51 \pm 6$ | $66 \pm 17$ |
| $R_{shunt}$(Ω cm$_2$) | $19 \pm 1$ | $1000 \pm 500$ | $110 \pm 60$ | $600 \pm 400$ |
| $\eta$(%) | $4.1 \pm 0.2$ | $3.2 \pm 0.2$ | $0.98 \pm 0.02$ | $0.7 \pm 0.2$ |

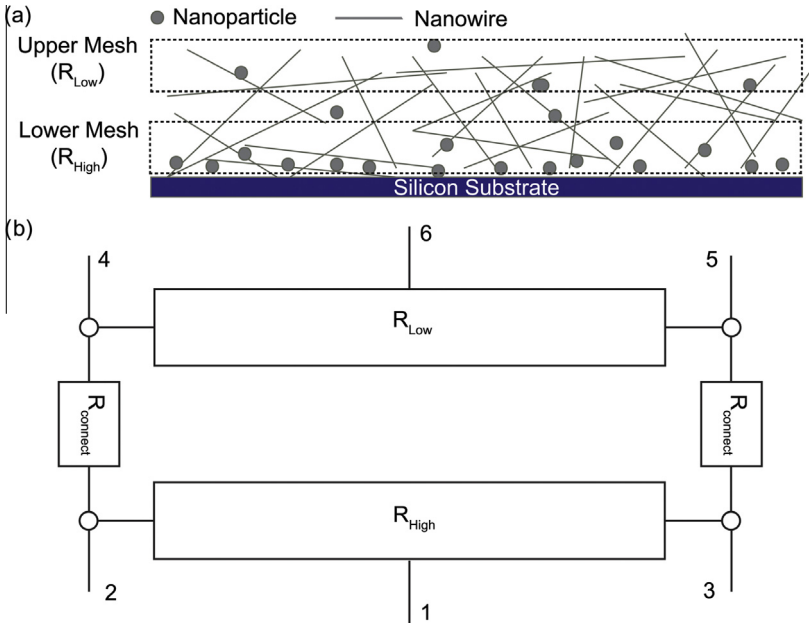


Fig. 8. (a) Diagram of potential layer formation of nanowire mesh with increased deposition cycles. (b) Circuit diagram of 3D mesh layers. Both sheet resistance and series resistance of Si15 sample measured between points 2 and 3. Sheet resistance of Si18 and Si21 measured between points 4 and 5. Series resistance of Si18 and Si21 can potentially be taken between points 1, 2, 3 and points 4, 5, 6 with a large number of possibilities for $R_{connect}$.

Table 3
Volumes of silver used per $cm^2$ for SP and AgNW electrodes including separate values for nanowires and nanoparticles of AgNW electrodes.

| Electrode component | Silver volume per $cm^2$ ($cm^3$) |
|---|---|
| SP grid fingers | 0.56 |
| Nanowires | $0.087 \pm 0.009$ |
| Nanoparticles | $0.066 \pm 0.008$ |
| Nanowires and nanoparticles | $0.15 \pm 0.01$ |

result in a volume $0.087 \pm 0.009$ $cm^3$ of silver, or ~16% of the volume used in SP grids. This is a large reduction in silver which could result in a large cost reduction.

### 3.7. Considerations between AgNW and silver grids

From the literature on SP silver grids there are some other factors that need to be considered for replacing silver grids with AgNW meshes. Silver pastes used in the SP process have a 70–85% silver content (Caballero, 2010). Other inclusions are organic compounds used as a solvent for the paste and to allow adherence between the silver after it has been SP. The final compound which is of more importance when considering using AgNWs instead is the glass frits. The glass frits allow contact to be made between the silver and the emitter layer of the cell by reducing the melting temperature of the passivation di-electric layer (Caballero, 2010; Schubert et al., 2003). When considering the use of silver nanowires it would be difficult to replicate this step with AgNW. This could also be a limiting factor in the series resistances observed in this work. One option of improving the contact between the AgNW mesh and the substrate could be the annealing temperature used, with a higher temperature improving the contact.

## 4. Conclusion

AgNW electrodes are observed to show favourable plasmonic behaviour when used in conjunction with crystalline silicon solar cells with an average of 22% more light transmission when compared to the non-AgNW shaded area of the silicon substrate, which is largely attributed to increased scattered transmission. Whilst a peak in IPCE was observed at the plasmonic resonance of the AgNWs overall the electrical properties of the c-Si with AgNWs were reduced compared to the cell without AgNWs. This is attributed to poor contact between the AgNW and the silicon substrate and overall poor light transmission through the mesh due to a high proportion of nanoparticles. It was observed that a large reduction in silver used in the nanowire meshes compared to the screen printed grids could be very favourable in reducing the cost of crystalline silicon cells.

## References

Braun, E. et al., 1998. DNA-templated assembly and electrode attachment of a conducting silver wire. Nature 391 (6669), 775–778.
Caballero, L.J., 2010. Contact definition in industrial silicon solar cells. Sol. Energy, 375–398.
Caswell, K.K. et al., 2003. Seedless, surfactantless wet chemical synthesis of silver nanowires. Nano Lett. 3 (5), 667–669.
Catchpole, K.R. et al., 2008. Plasmonic solar cells. Opt. Exp. 16 (26), 21793–21800.
Catrysse, P.B., Fan, S., 2010. Nanopatterned metallic films for use as transparent conductive electrodes in optoelectronic devices. Nano Lett. 10 (8), 2944–2949.
Chen, C.C. et al., 2012a. Visibly transparent polymer solar cells produced by solution processing. Acs Nano 6 (8), 7185–7190.

Chen, T.G. et al., 2012b. Flexible silver nanowire meshes for high-efficiency microtextured organic-silicon hybrid photovoltaics. ACS Appl. Mater. Interfaces 4 (12), 6857–6864.
Gaynor, W. et al., 2009. Fully solution-processed inverted polymer solar cells with laminated nanowire electrodes. ACS Nano 4 (1), 30–34.
Govindaraj, A. et al., 2000. Metal nanowires and intercalated metal layers in single-walled carbon nanotube bundles. Chem. Mater. 12 (1), 202–205.
Han, Y.-J. et al., 2000. Preparation of noble metal nanowires using hexagonal mesoporous silica SBA-15. Chem. Mater. 12 (8), 2068–2069.
Hilali, M.M. et al., 2004. A review and understanding of screen-printed contacts and selective-emitter formation. In: 14th Workshop on Crystalline Silicon Solar Cells and Modules, vol. 1617, pp. 80401–3393.
Hong, B.H. et al., 2001. Ultrathin single-crystalline silver nanowire arrays formed in an ambient solution phase. Science 294 (5541), 348–351.
Hu, J.Q. et al., 2004. A simple and effective route for the synthesis of crystalline silver nanorods and nanowires. Adv. Funct. Mater. 14 (2), 183–189.
Hutter, E., Fendler, J.H., 2004. Exploitation of localized surface plasmon resonance. Adv. Mater. 16 (19), 1685–1706.
Jana, N.R. et al., 2001. Wet chemical synthesis of silver nanorods and nanowires of controllable aspect ratio. Chem. Commun. (7), 617–618
Kang, M.-G., Guo, L.J., 2007. Nanoimprinted semitransparent metal electrodes and their application in organic light-emitting diodes. Adv. Mater. 19 (10), 1391–1396.
Korte, K.E. et al., 2008. Rapid synthesis of silver nanowires through a CuCl or CuCl2-mediated polyol process. J. Mater. Chem. 18 (4), 437–441.
Kottmann, J., Martin, O., 2001. Coupling in metallic nanowires. Numer. Study 8 (12), 655–663.
Morgenstern, F.S.F. et al., 2011. Ag-nanowire films coated with ZnO nanoparticles as a transparent electrode for solar cells. Appl. Phys. Lett. 99 (18), 183307–183307.
Murphy, C.J., Jana, N.R., 2002. Controlling the aspect ratio of inorganic nanorods and nanowires. Adv. Mater. 14 (1), 80.
Rowell, M.W. et al., 2006. Organic solar cells with carbon nanotube network electrodes. Appl. Phys. Lett. 88 (23), 233506.
Schubert G. et al., 2003. Current transport mechanism in printed ag thick film contacts to an n-type emitter of a crystalline silicon solar cell, in: PVSEC-14 Proceedings, pp. 441–442.
Sun, Y. et al., 2002. Crystalline silver nanowires by soft solution processing. Nano Lett. 2 (2), 165–168.
Temple, T. et al., 2009. Influence of localized surface plasmon excitation in silver nanoparticles on the performance of silicon solar cells. Sol. Energy Mater. Sol. Cells 93 (11), 1978–1985.
Tung, V.C. et al., 2009. Low-temperature solution processing of graphenecarbon nanotube hybrid materials for high-performance transparent conductors. Nano Lett. 9 (5), 1949–1955.
Underwood, S., Mulvaney, P., 1994. Effect of the solution refractive index on the color of gold colloids. Langmuir 10 (10), 3427–3430.
van de Groep, J. et al., 2012. Transparent conducting silver nanowire networks. Nano Lett. 12 (6), 3138–3144.
Wohlgemuth, J.H. et al., 1990. Cost effectiveness of high efficiency cell processes as applied to cast polycrystalline silicon. Photovoltaic Specialists Conference, 1990. In: Conference Record of the Twenty First IEEE. IEEE, pp. 221–226.
Zhou, Y. et al., 1999. Formation of silver nanowires by a novel solid–liquid phase arc discharge method. Chem. Mater. 11 (3), 545–546.